Front. Optoelectron. 2014, 7(1): 1–19
DOI 10.1007/s12200-014-0387-5

REVIEW ARTICLE

Recent advances in development of vertical-cavity based short pulse source at 1.55 μm

Zhuang ZHAO (✉), Sophie BOUCHOULE, Jean-Christophe HARMAND, Gilles PATRIARCHE, Guy AUBIN, Jean-Louis OUDAR

Laboratoire de Photonique et de Nanostructures (LPN), CNRS, Marcoussis, France

Abstract This paper reviews and discusses recent developments in passively mode-locked vertical external cavity surface emitting lasers (ML-VECSELs) for short pulse generation at 1.55 μm. After comparing ML-VECSELs to other options for short pulse generation, we reviewed the results of ML-VECSELs operating at telecommunication wavelength and point out the challenges in achieving sub-picosecond operation from a ML-VECSEL at 1.55 μm. We described our recent work in the VECSELs and semiconductor saturable absorber mirrors (SESAMs), their structure design, optimization and characterization, with the goal of moving the pulse width from picosecond to sub-picosecond.

Keywords semiconductor laser, vertical external cavity surface emitting laser (VECSEL), indium phosphide, heat dissipation, saturable absorber mirror, mode-locking

1 Introduction

Laser sources emitting short pulses are now widely employed in many scientific applications such as waveform measurement, time-resolved spectroscopy, frequency combs, optical interconnection and ultra-high capacity telecommunication systems. Numerous laboratory experiments have confirmed that short laser pulses can significantly improve existing applications, for example, increase telecommunication data rates [1] and improve computer interconnects [2], or control the optical clocking of microprocessors [3]. Today, telecommunication systems rely on externally modulated continuous-wave semiconductor lasers. With the combination of wavelength division multiplexing (WDM) technology, transmission rates of more than 1 Tbit/s have been demonstrated [4]. Ultrafast lasers can be used as pulse sources in the telecommunication system, rather than shaping the pulses by modulator. The short pulse duration, high peak power, wide spectral bandwidth and low timing jitter translate into simplified synchronization and improved receiver sensitivity [5]. Optical analog-to-digital conversion is another application of short optical pulses. Short pulses perform the sampling of an optical signal in a nonlinear medium to avoid requiring a very fast photodetector [6].

Several options are possible for the generation of short pulses in the telecom window (1.3 – 1.55 μm). They present different advantages in terms of pulse energy, timing jitter, repetition rate, and tunability of the repetition rate. To date, multi-gigahertz pulse sources have involved an edge-emitting semiconductor laser, which is usually either actively or hybridly mode-locked. Typically, the same epitaxial layer forms both the gain (with a forward-biased section) and the saturable absorber (with a reverse-biased section) in ultrafast edge-emitting semiconductor lasers. Such mode-locked edge emitting lasers are attractive because they are compact and potentially integratable with other photonic devices on a single chip. In 1985, Lau et al. reported one of the first attempts to mode lock a monolithic 1.97 mm long GaAlAs laser, which produced stable pulses at 17.7 GHz repetition rate [7]. Very stable pulse trains at 40 to 80 GHz repetition frequency, and the pulse width of 1 to 2 ps have been demonstrated, for example by HHI (Germany) from multi-quantum well (MQW) multi-section edge emitting lasers [8]. More recently, the PHOTEL group at LPN demonstrated pulse generation at this wavelength from a two-section quantum dots based laser at a very high repetition frequency (346 GHz) [9]. Unfortunately, it appears difficult to achieve high average power from such lasers, while keeping good passive mode-locking performances. The typical average output power from mode-locked quantum dot edge emitting lasers at 1.55 μm is in the sub-mW range.

Received October 24, 2013; accepted November 27, 2013

E-mail: zhuang.zhao@lpn.cnrs.fr

In addition, owing to the geometry of such edge emitting lasers, the profile of the emitted beam is strongly asymmetric. It is also quite challenging to fabricate a monolithic edge-emitting laser with a very precise pulse repetition rate, because a very precise control of cavity length is difficult.

Diode-pumped fiber pulse lasers have been developed and offer excellent performance. Actively mode-locked erbium doped fiber lasers with long, dispersion-compensated cavity have produced harmonically mode-locked pulses used in 1.28 Tbit/s optical time-division multiplexing (ODTM) systems [10]. However, multi-gigahertz fiber lasers require sophisticated means to obtain stable harmonic mode-locking because they have many pulses in the long fiber cavity. Additionally, individual pulses generated by harmonic mode-locking do not necessarily exhibit a fixed phase relation. This excludes promising and important modulation formats, such as return-to-zero differential phase shift keying [11]. In order to operate a fiber laser at multi- gigahertz fundamental repetition rates, extremely short active fibers have to be used, which is at the expense of power efficiency. Recently, an all-fiber passively mode-locked laser operating at record fundamental repetition rate of 20 GHz has been demonstrated, based on a 5 mm long cavity with a highly doped Er^{3+}:Yb^{3+} fiber and a fiber compatible carbon nanotube based saturable absorber (CNT-SA) [12].

Two other interesting kinds of pulse lasers are based on passive mode-locking mechanism: passively mode-locked solid state laser and passively mode-locked vertical external cavity surface emitting lasers (ML-VECSELs). Passive mode-locking mechanism means that the pulses are generated without using any expensive multi-gigahertz electronics. In addition, the pulses may originate from fundamental mode-locking even at multi-GHz rate. Thus, every output pulse is a copy of the same single pulse, which travels back and forth in the cavity. Therefore, pulse-to-pulse variations are minimized and the phase of the pulses is constant. As for the repetition frequency tunability, the external cavity laser allows for tuning the repetition rate of pulses mechanically by adjusting the cavity length. Monolithic lasers and fiber based laser have a more limited tuning range because the change in cavity length is induced by a change of refractive index. The Keller's group at ETH has developed passively mode-locked solid state lasers with very good pulse quality, comparatively high output powers, and high pulse repetition rates [13]. A fundamental repetition rate up to 100 GHz has been demonstrated with a diode-pumped mode-locked Er:Yb:glass laser at 1.5 μm [14]. However, only a few solid-state gain media are available in the telecom wavelength ranges. Fortunately, passively mode-locked VECSEL formed a new step to bridge the gap between semiconductor lasers and solid-state lasers: it combines the versatility of a semiconductor quantum well gain medium with the capacity of power scalability with a diffraction limited output beam, fundamental mode-locking at multi-GHz rate and repetition frequency tunability.

This paper reviews and discusses picosecond to sub-picosecond pulse generation from mode-locked 1.55-μm VECSELs. Starting from an overview of different short pulses sources, the motivation for passively mode-locked optically pump vertical external cavity semiconductor laser (OP-VECSEL) device development is presented. A brief overview of the state-of-the-art for mode-locked VECSELs is presented in Section 2, focusing on devices operating close to 1.55 μm. Section 3 focuses on the design, fabrication and characterization of optically-pumped VECSELs, with a particular emphasis on the thermal management. Section 4 discusses our development of dispersion managed semiconductor saturable absorber mirrors (SESAMs) for mode-locking. In Section 5, we present the mode-locking experiments with the thermally-optimized VECSEL chip assembled with the different dispersion-managed SESAMs. Finally, Section 6 gives the conclusions and outlook.

2 State-of-the-art of mode-locked VECSEL

The first passively mode-locked OP-VECSEL was demonstrated in 2000 [15], by Hoogland et al. in Anne Tropper's group at the University of Southampton. In the following years, large progress has been made. Figure 1 presents a summary of the results reported to date for mode-locked VECSELs operating in the near infrared range. The results are presented as a function of pulse repetition rate and pulse duration, two important parameters of optical pulse sources.

The groups of Prof. Keller at ETH Zurich and Prof. Tropper at University of Southampton have made key contributions to this field, and most of the state-of-the-art results obtained at 1 μm wavelength from GaAs-based

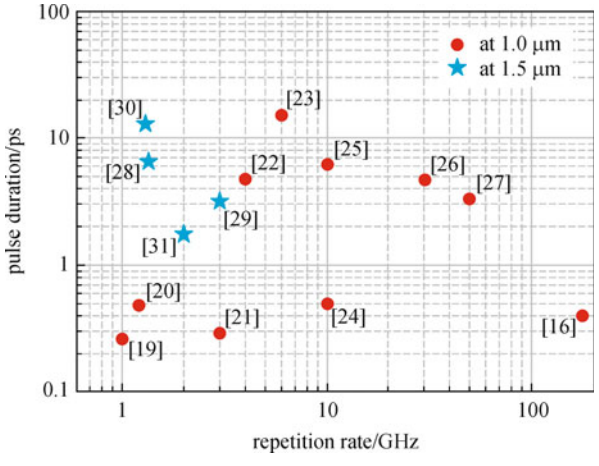

Fig. 1 Summary of mode-locked pulse characteristics obtained from mode-locked VECSELs in near infrared range

VECSELs and shown in Fig. 1 have been reported by these two groups. Today, the performances of mode-locked VECSELs operating around 1 μm are impressive: a pulse repetition rate of 175 GHz [16], pulse duration of 60 fs [17] and an average output power of 6.4 W with a mode-locked integrated external-cavity surface emitting laser (MIXSEL) [18].

As a main conclusion of Fig. 1, sub-picosecond pulses have already been obtained at various repetition rates at 1 μm [16,19–27]. In contrast, there are only very few results for mode-locked VECSEL at 1.5 μm. The group of Prof. Tropper has reported the first picosecond pulse generation from a 1.5 μm passively mode-locked VECSEL in 2003 [28]. The quantum well gain structure used in this laser consisted of an InGaAsP quantum well active region on the top of an InP/InGaAsP distributed Bragg reflector (DBR) grown on InP substrate. The SESAM was also grown on InP. The authors demonstrated 6.5 ps pulses with an average power of 13.5 mW at a fundamental repetition frequency of 1.34 GHz. The operating temperature was of −8°C. The group of Prof. Larsson at Chalmers University in Sweden has developed a fast GaInNAs SESAM operating at 1.55 μm and demonstrated in 2005 stable mode-locked nearly transform-limited pulses with pulse width of 3.2 ps, a repetition rate of 2.97 GHz and an average power of 120 mW [29]. The heating in the VECSEL chip was reduced by using a 50-μm thick diamond heat spreader bonded to the VECSEL surface. Finally, Prof. Okhotnikov's group demonstrated very recently with its collaborators at EPFL the first high-power passively mode-locked VECSEL operating at 1.57 μm wavelength [30]. Efficient heat removal from the gain section was mainly obtained by using an intra-cavity diamond etched with a wedge and an excellent antireflection coating deposited on the heat spreader surface. The mode-locked laser produced more than 0.6 W of average output power at a heat sink temperature of 15°C. The pulse width was of 16 ps in this experiment [30].

In 2010, our group demonstrated a picosecond pulse generation from a 1.55 μm mode-locked VECSEL operating at room temperature [31]. The laser operated at a repetition frequency of 2 GHz and emitted near-transform-limited 1.7 ps pulses with an average output power of 15 mW. The SESAM was grown on GaAs with an absorbing region consisting of a single GaInNAs quantum well, while the VECSEL relied on the downward heat sinking approach which will be explained in detail in Section 3.1. This was the shortest pulse width, but sub-picosecond pulse generation still had to be demonstrated. Progress toward ultrashort pulse generation at 1.55 μm is difficult because of the lack of fast SESAMs at this wavelength, and also because of the low power performance of the gain chip mainly due to the bad thermal behavior of quaternary InP-based semiconductor compounds.

3 VECSEL gain chip

A VECSEL chip is formed by a stack of semiconductor thin layers. The semiconductor chip consists of two sections: a highly reflecting mirror, and the active region. The typical structure of a VECSEL is illustrated in Fig. 2. It shows the conduction and valence band energy levels across the semiconductor layers and explains the functions of the various layers. The highly-reflecting (HR) mirror incorporates a periodic quarter-wave stack of layers of alternating high and low refractive index. Such a DBR acts as a HR plane cavity mirror. In front of the DBR is the

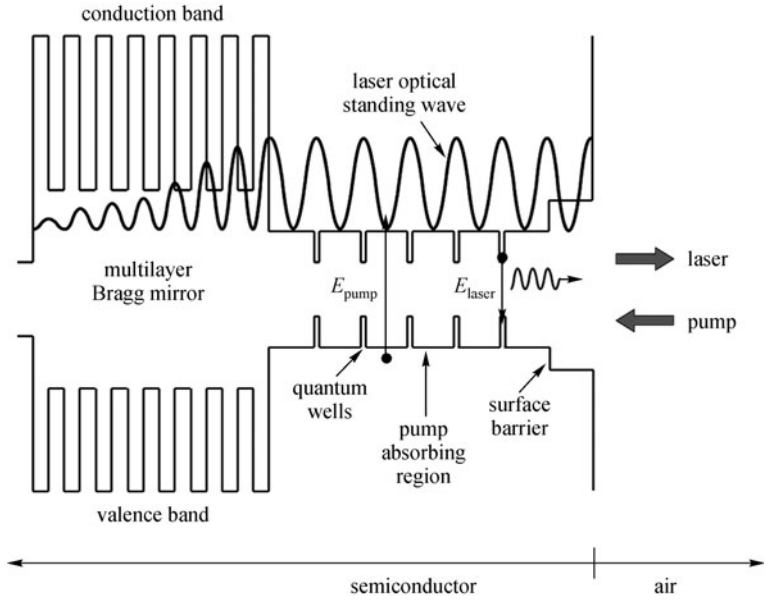

Fig. 2 Typical structure of an optically pumped VECSEL [32]

active region, which is typically a few half wavelengths in thickness, and contains quantum wells. When a pump laser is focused on the surface, the semiconductor chip absorbs the pump light and converts it into desired laser light. The optical wave of the laser mode, back-reflecting from the DBR, sets up a standing wave inside the chip due to the microcavity effect. Quantum wells have to be placed near the antinodes of this standing wave in order to provide efficient gain to the laser. Typically, the gain region spreads over several periods of this standing wave.

3.1 State-of-the-art at 1.5 μm

1.55 μm VECSELs make use of an InP-based active region, generally including InGaAsP or InGaAlAs quantum wells having a high optical gain in this spectral region. Optical pumping is moreover an easy method to achieve a homogenous inversion of population over a large area and thus allows for producing intense, high quality beam from a VECSEL. In this way, several tens of Watts are obtained today in the near infrared around 1 μm from GaAs-based OP-VECSELs [33]. On the other hand, the thermal conductivity of quaternary materials used in InP based devices is really poor compared to that of GaAs based devices emitting around 1 μm. The excessive heating in the active region arising in InP-based 1.5 μm structures generally limits the maximum output power. Thus, efficient heat dissipation from the active region is crucial in 1.5 μm VECSELs. Table 1 shows some results demonstrated to date from OP-VECSELs operating around 1.5 μm with different thermal management schemes: intra-cavity heat spreader and downward heat dissipation. These two approaches will be further analyzed by thermal modeling in Section 3.2. Using intra-cavity heat spreader, most of the heat generated in the active region is spread out in the heat spreader, and therefore by-passes the thermal impedance of the DBR and substrate. Downward heat dissipation technique relies on removing the heat through the DBR and substrate.

The group of Prof. Larsson at Chalmers University of Technology in Sweden was one pioneer in the field of 1.5 μm OP-VECSEL. They first demonstrated in 2004 a maximum output power of 70 mW at 233 K (~ −40°C) from an InP-based OP-VECSEL in continuous wave (CW) operation at 1550 nm [34]. Their VECSEL chip was grown on a bulk InP substrate and included five groups of four InGaAsP quantum wells on top of a 48 period InP/InGaAsP DBR. In a second step, they reduced the thermal impedance of the VECSEL chip by using an intra-cavity heat spreader bonded to the VECSEL surface. They used a Silicon substrate as the heatspreader [38], and finally selected a 50 μm thick type IIa natural diamond [35]. The diamond with a typical size of 5 mm × 5 mm was bonded to the surface of a 4 mm × 4 mm VECSEL chip by the technique of liquid capillary bonding. Using this approach, they demonstrated in 2004 an output power exceeding 470 mW at a heat sink temperature of 0°C, while an output power of 170 mW could be obtained at room temperature [35].

Still using the intra-cavity heat spreader approach, the group of Prof. Okhotnikov at Tampere University of Technology in Finland, in collaboration with Dr. Sirbu and coworkers at EPFL in Switzerland, reported in 2008 a record output power of 2.6 W from a 1.57 μm OP-VECSEL [36]. Their VECSEL configuration is shown in Fig. 3(a). The active region comprised 5 groups of 2 AlGaInAs quantum wells. They replaced the InP-based DBR by a 35-pair AlGaAs/GaAs DBR with better thermal conductivity, assembled with the InP-based active region by wafer fusion. In addition, a 300 μm thick intracavity natural type IIa diamond heat spreader (size of 3 mm × 3 mm) was bonded to the top surface of the sample by capillary bonding. As can be seen in Fig. 3(a), a special care was also taken in mounting the laser chip: the sample is pressed between two copper plates with indium foil to ensure reliable contact between the surfaces. The topmost metal plate had a circular aperture for signal and pump beams. The bottom copper plate on top of which the VECSEL was placed was cooled by a Peltier element. The hot face of the Peltier was in contact with a water cooled copper block as the heat sink.

It can be concluded that the intra-cavity heat spreader approach is an efficient solution for 1.55 μm OP-VECSEL operating in CW regime with high output power. However,

Table 1 Summary of main results obtained with 1.55 μm OP-VECSELs

λ_0/nm	active region (quantum wells)	bottom mirror	P_{out}/W	heat spreader (HS) or downward heat dissipation (DHD)	operating temperature/K	reference (date)
1550	20 InGaAsP	48-pair InP/InGaAsP	0.07	DHD	233	[34] (2004)
			0.8	HS	240	[35] (2004)
1570	10 InGaAlAs	35-pair GaAs/AlGaAs	2.6	HS	283	[36] (2008)
1550	8 InGaAlAs	hybrid 17-pair GaAs/AlGaAs-gold mirror	0.07	DHD	298	[37] (2008)

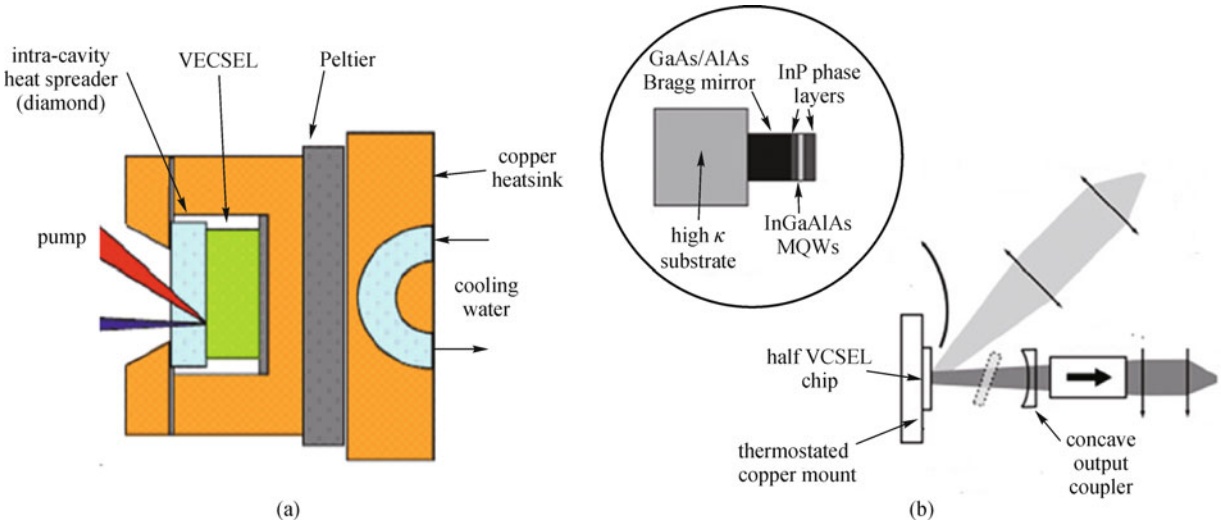

Fig. 3 Schematics of thermal management techniques. (a) Intra-cavity heat spreader approach (after Ref. [36]); (b) downward heat dissipation approach (after Ref. [37])

the intra-cavity heat spreader also acts as a Fabry-Perot etalon. It may introduce an unwanted spectral selection limiting the minimum pulse-width in the mode-locking regime. Moreover, it is not easily compatible with non-perfectly plane VECSEL surface.

An alternative to the intra-cavity heat spreader is the downward heat sinking approach. At LPN, we investigated this second approach for the development of 1.55 μm mode-locked VECSELs. In a first report in 2008 [37], we compared different kinds of bottom DBR and substrates. Figure 3(b) shows the VECSEL configuration that was used. A single-mode output power of 77 mW (limited by the available pump power) was obtained under CW laser operation at room temperature.

3.2 Thermal optimization of VECSEL

Thermal simulations have been carried out using Comsol Multiphysics (2D model). Parameters used in the simulation are given in Table 2. The heat conduction equation is solved for a circularly symmetric device and the semiconductor structure is simplified into three parts: a top phase layer, the active region and the bottom DBR mirror. The active region is made of InGaAlAs. It includes 8 compressively strained InGaAlAs quantum wells embedded in a lattice-matched InGaAlAs absorbing layer, and will be further described in Section 3.3. In the following simulations, the InP-based part of the VECSEL structure (i.e., top phase layer and active region) is kept unchanged for comparison purpose. The geometry used for the modeling of VECSEL chip with a top mounted heatspreader is schematically depicted in Fig. 4. The geometry used for modeling of VECSEL chip based on the downward heat sinking approach is depicted in Fig. 5. In the latter case, the host substrate consists either of chemical vapor deposition (CVD) diamond, copper, or gold. Bulk host substrates can be assembled with the semiconductor chip via an $AuIn_2$ metallic layer, and the assembly procedure will be detailed in Section 3.3. The VECSEL chip is placed on a temperature-regulated copper heat sink with an intermediate in foil to improve the thermal contact. All the thermal conductivities are kept constant and equal to the values at 300 K and internal interfaces are perfectly conducting. Additionally, the average thermal conductivity of DBR mirror is calculated in both radial (κ_r) and longitudinal (κ_z) axis. As for the boundary conditions in the longitudinal direction, the bottom part of the heatsink is kept at a constant temperature while the top surface of the structure is considered as thermally insulated (air convection is neglected). In radial direction, symmetry boundary conditions are used at the axis of rotation. Radius of VECSEL chips are set to 2 mm in the simulations, which is at least 12 times larger than the pump spot radius. In this case, thermal insulation is assumed at the edge of VECSEL chips. Pump absorption and hence heat loading is assumed to occur mainly in the active region, but also to some extent in the bottom mirror [40,41]. Diode laser pumping with a Gaussian profile at 980 nm is assumed. The linear absorption coefficients in the different layers at this wavelength are given in Table 2. The fraction of pump power absorbed in the active region and converted to heat is 0.37 [40]. The temperature rise in the active region has been calculated as a function of pump spot radius for a fixed average pump power density of 10 kW/cm^2.

VECSELs associated to a 300 μm thick intracavity diamond heatspreader have first been considered as a thermal reference [30,41,42]. VECSELs with the same InP-based active region but with different bottom Bragg mirrors and substrates have then been considered: a 48-pair InP/InGaAsP Bragg mirror on InP substrate [42], a 35-pair

Table 2 Thermal conductivity values and layer thickness used in the thermal simulations. (*): As the pump power has been completely absorbed after the Au layer in the mirror, the absorption coefficient was set to zero in the simulation

layers	average thermal conductivity/$(W\cdot(K\cdot m)^{-1})$	absorption coefficient at the pump wavelength/cm^{-1}	layer thickness/μm
heatspreader	2000	0	300
InP phase layer	68	0	1.1
quartenary active region	4.5	1.5×10^4	0.7
48-pair InP/InGaAsP DBR	$\kappa_r = 38.5$, $\kappa_z = 12.7$	0	11.3
35-pair GaAs/AlGaAs DBR	$\kappa_r = 74.4$, $\kappa_z = 69.9$	20	9.3
17-pair GaAs/AlGaAs DBR	$\kappa_r = 74.4$, $\kappa_z = 69.9$	20	4
InP substrate	68	0	300
GaAs substrate	55	0 (*)	300
CVD diamond	2000	0	300
copper	400	0 (*)	varied
Au	300	1.3×10^6	150
$AuIn_2$	162	0 (*)	0.4
In	81	0 (*)	50
Cu heatsink	400	0 (*)	1000

GaAs/AlGaAs Bragg mirror on GaAs substrate [30], and the limit case with no Bragg mirror nor substrate. In Fig. 4 showing the geometry used in modeling, the vertical yellow dash on the right side of the structure indicates the thermal short-cut (made of copper) between bottom and top heatsink. Results in Fig. 4 reveal that for pump spot radius up to 150 μm the heat dissipation mostly occurs through the top-mounted natural diamond when it is used as intra-cavity heat spreader. The thermal impedance of the bottom Bragg mirror and of the substrate in the VECSEL chip has a negligible impact on the temperature increase in the active layer in this case. A temperature rise lower than 10 K is systematically calculated (10 kW/cm^2 pump power density) for a pump spot radius up to 150 μm.

An alternative to the intra-cavity heat spreader is the downward heat dissipation scheme. In the downward heat sinking approach, the thermal impedance of the bottom mirror and substrate becomes of paramount importance. We have already demonstrated the low thermal impedance of a hybrid metal (Au) -metamorphic GaAs/AlGaAs mirror associated to a highly thermally-conductive CVD diamond host substrate [31,37]. The thermal performance of such a VECSEL structure is illustrated in Fig. 5. The same active region as for the calculations of Fig. 4 is considered, but is combined with a 17-pair GaAs/$Al_{0.97}Ga_{0.03}As$-Au hybrid mirror, associated to a CVD diamond host substrate via metallic bonding, or to an integrated metallic (Cu, Au) substrate. For pump spot radii larger than 20 μm, the CVD diamond substrate leads to superior performance with a significant reduction of the temperature rise in the active region. Moreover, a quasi-one-dimensional heat flow can be observed in this case for large pump diameters, of particular interest for power-scaling. Results of Fig. 5 also demonstrate that a cost-effective version consisting in the use of a Cu host substrate, will also lead to low temperature increase for VECSELs with pump radii in the range of 20–4 μm. $\Delta T \leqslant 20$ K is obtained even for radius up to 100 μm. It was shown experimentally that the thermal roll-over effect occurs typically for temperature rise of ~30 K in the *L-I* curve for electrically-pumped 1.55 μm VECSELs with similar active region [43]. We have performed a detailed study of the thermal performances of VECSELs with a copper substrate in collaboration with Sirbu and coworkers [39]. Our simulation results showed that the copper substrate thickness should be larger than ~ 80 μm for efficient heat dissipation for pump spot radius in the 30 – 50 μm range.

3.3 VECSEL fabrication

The InP-based epitaxial structure has been grown on InP wafer using metal-organic vapor-phase epitaxy (MOVPE) at Alcatel-Lucent 3-5 Laboratory, France. The whole VECSEL fabrication process is shown in Fig. 6.

In step (1), the InP-based 2λ-thick active region, grown on an InP substrate, includes eight strained InGaAlAs quantum wells distributed among three optical standing-wave antinode positions. Etch-stop layers grown on top of the InP substrate enable the removal of the InP substrate, resulting in an active region directly in contact with the host substrate.

In step (2), the 17-pair GaAs/$Al_{0.97}Ga_{0.03}As$ semiconductor Bragg mirror is integrated to the active region by metamorphic growth using molecular beam epitaxy (MBE) [31]. Another integration technique is wafer fusion, successfully developed for GaAs-based DBR and InP-

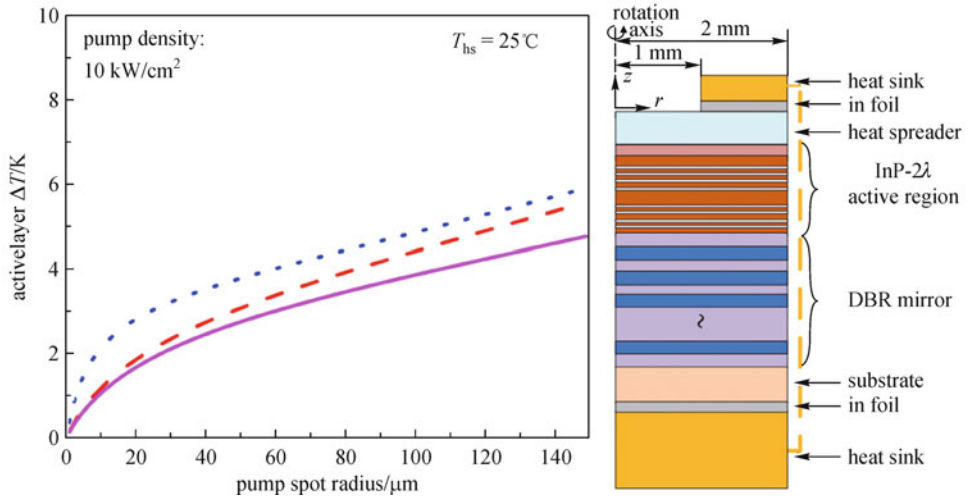

Fig. 4 Temperature rise in active layer calculated versus pump spot radius for 300 μm diamond heat spreader and with different DBRs and substrates: 35-pair GaAs/AlGaAs DBR mirror on GaAs substrate (red dash), and 48 pairs InP/InGaAsP DBR mirror on InP substrate (blue dot). The limit case of the active region directly bonded onto the same heat spreader is a reference (magenta line) [39]

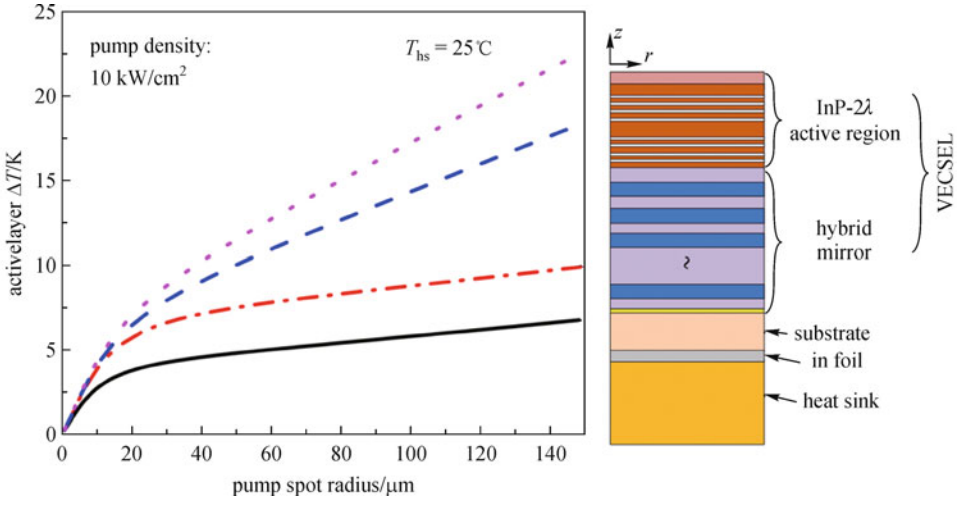

Fig. 5 Temperature rise in active region calculated versus pump spot radius for a hybrid GaAs/AlGaAs-gold mirror with different host substrates: 300 μm thick CVD diamond (red dash dot), 150 μm thick copper (blue dash), and 150 μm thick gold (magenta dot). The limit case of the active region directly bonded onto 300 μm diamond host substrate with no bottom mirror nor substrate is also reported as a reference (black line) [39]

based active region by EPFL [39,44]. From temperature calculation in the active region of 1.55 μm VECSELs, we have shown that the InP-based quaternary alloys (InGaAsP or InAlGaAs) that form the DBR is hampered by the very low thermal conductivity of these materials, resulting in high thermal impedance. One solution to this problem consists in replacing the as-grown InP-based DBR with a GaAs/AlGaAs DBR with better thermal conductivity.

Due to the large lattice mismatch between InP and GaAs, misfit dislocations form in the epitaxial layers at the InP/GaAs interface during the metamorphic regrowth of the GaAs/AlGaAs DBR of top of InP. The threading dislocations originating from the hetero-interface can propagate into the GaAs/AlAs DBR and possibly induce defects in the InP-based active layer, thus degrading the performance of the laser. Figure 7 shows a typical bright-field (BF) scanning transmission electron microscopy (STEM) image of the InP/GaAs interface. The TEM slice was formed in the structure at the end of the full VECSEL process. STEM observations show a gradual decrease of dislocation density in GaAs/AlAs DBR: (7~9) × 10^{10} cm^{-2} close to the interface, (2~3) × $10^{10}cm^{-2}$ in the third layer from the interface, and ~ 10^{8} cm^{-2} in the last GaAs layer. However, the abruptness and flatness of the GaAs/AlGaAs epitaxial interfaces, of critical importance for the Bragg mirror, is maintained. On the other hand, no structural

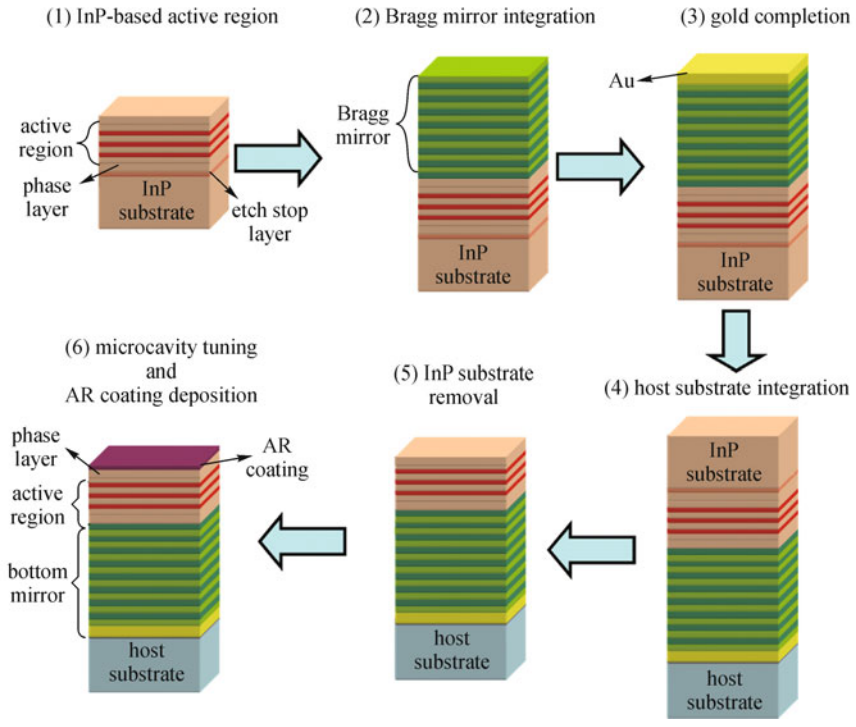

Fig. 6 Fabrication process of VECSEL chips

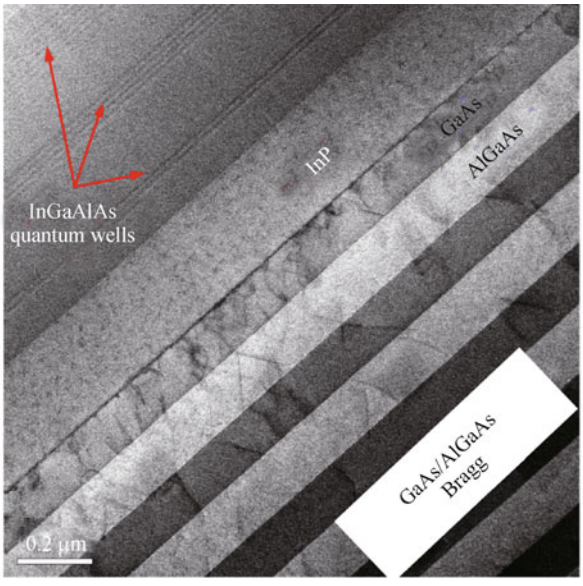

Fig. 7 BF-STEM image of interface between InP-based active structure and metamorphic GaAs/AlGaAs DBR regrown by MBE [45]

degradation of the InP-based active region can be detected. This has been confirmed by time-resolved photoluminescence (PL) measurements showing no increase of non-radiative lifetime.

Then, an additional 150 nm-thick Au layer is deposited on the surface of the Bragg mirror to enhance the bottom mirror reflectivity (step (3)). The semiconductor chip with deposited gold is then integrated to a CVD-diamond host substrate in step (4). In step (5), the InP substrate is removed by both mechanical polishing and wet selective etching at room temperature. Finally in step (6), the InP phase layer is etched and the anti-reflection (AR) coating at 980 nm is deposited, so that the position of the resonant half-cavity mode of the VECSEL chip is close to the gain maximum after AR layer deposition.

3.4 Thermal and CW lasing performances

The VECSEL is tested in a simple plane-concave cavity configuration as previously detailed [37]. Figure 8 shows that the VECSEL chip is mounted onto a copper heatsink to control the temperature of the device with a Peltier module. The chip is pumped with a CW fiber-coupled 980 nm multimode laser diode delivering up to 6 W focused on approximately a ~100 μm diameter spot with incidence angle of 45°. The pump spot radius is estimated by an InGaAs camera with a typical spatial resolution of ~ 10 μm. This high power multimode pump is used to evaluate the ultimate performance of the VECSEL with diamond substrate. The external cavity is formed by the VECSEL chip and a concave dielectric mirror with reflectivity of 99% at 1550 nm and curvature radius of 25 mm. The overall cavity length is around 25 mm. Figure 9 displays the lasing performance of this VECSEL at two different heatsink temperatures. At a fixed heatsink temperature of 0°C with water cooling system, the obtained output power

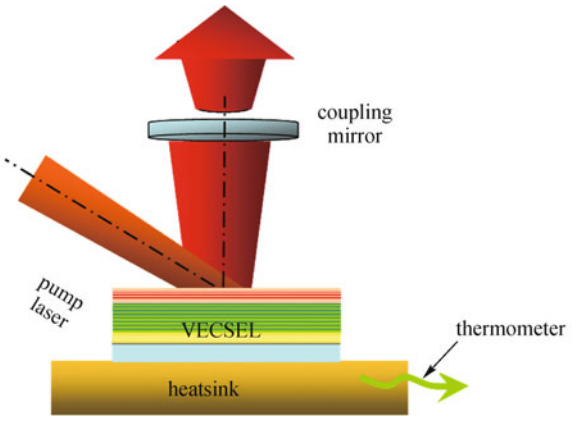

Fig. 8 VECSEL plane-concave cavity setup. The VECSEL chip is attached to a copper mount with heat conductive paste. The temperature of the copper plate is measured with a 10 kΩ thermistor. The copper plate temperature is regulated with a Peltier element, which is fixed to a heatsink. The heat is dissipated from the heatsink with a fan or with water cooling system

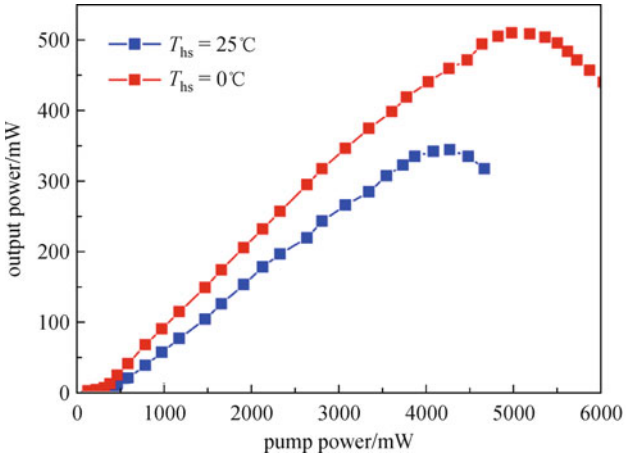

Fig. 9 CW emitted power of VECSELs with CVD-diamond host substrate versus incident pump power at different temperatures in the plane concave cavity configuration

is up to 510 mW thermal roll-over occurs, while it is limited to 350 mW at a heatsink temperature of 25°C.

4 SESAM

The development of SESAMs has been a key contribution to the generation of short pulses from ultrafast solid-state and semiconductor lasers [46,47]. A SESAM consists of a stack of epitaxially-grown semiconductor layers. SESAM structures can be epitaxially grown with a full control of their key design parameters – magnitude and phase of the optical absorption and reflection, adjustment of the saturation fluence (energy level where the device saturates). Moreover, the carrier recovery time (how fast the absorber recovers) can be tuned down to the picosecond range by modifying the non-radiative recombination lifetime with an appropriate design or by the optimization of the growth conditions. The modulation depth (maximum nonlinear change in reflectivity), the non-saturable loss (amount of permanent loss of the device), the saturation fluence and the carrier recovery time are the main characteristics of a SESAM, allowing to control the mode-locked pulse properties (pulse width, pulse chirp, etc) [13].

4.1 SESAM structure

The first SESAM was designed for resonant passive mode-locking (RPM) in 1990; the coupled cavity including the saturable absorber generates a rapid amplitude modulation that strongly induces mode locking [48]. Today, the typical structure of SESAM is a multi-layer stack which can be optimized depending on where exactly the saturable absorber material is placed inside this multi-layer system. The top reflector of the SESAM provides an adjustable parameter that determines the intensity of the stationary wave inside the SESAM microcavity and therefore the saturation fluence of the saturable absorber device. Thus, this design allowed for a large variation of absorber parameters by simply changing the absorber thickness and the top reflector. This resulted in the general concept of SESAM without any restrictions on the mirror design [13,49], sketched in Fig. 10.

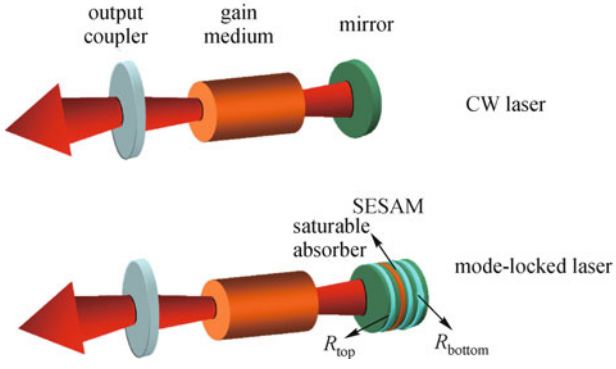

Fig. 10 General concept of SESAM without any restrictions on the mirror design [13]

4.1.1 Material requirement

To be useful as a SESAM absorber, the active semiconductor material must fulfill several requirements. First and most important is the short lifetime (in the picosecond range) of the excited carriers. To make the SESAM work with short pulses at high repetition rates, the equilibrium conditions in the absorbing layer have to be restored quickly after bleaching by a laser pulse. The bleaching is achieved by filling the available states in the conduction

band with photogenerated carriers, which leads to a saturation of the absorption until these carriers recombine. For SESAMs, carrier recovery times around 250 ps and below are desired to achieve pulse durations in the range of a few picoseconds [13,46].

Second, since SESAMs are intracavity elements, even small nonsaturable losses are undesirable, as they are enhanced strongly by its microcavity effect. The nonsaturable losses can result from the absorption related to the defects introduced by the nonradiative recombination centers. This means that SESAM fabrication technique should not change the nonsaturable loss too much when using fast nonradiative recombination with deep level defects. The techniques used for fast nonradiative recombination in SESAM, like low-temperature epitaxial growth, can achieve an ultrafast carrier recovery time, while resulting in large nonsaturable losses from the strong defect absorption [50]. The induced high nonsaturable loss will prevent the SESAM to be used in a mode-locked VECSEL. We review the techniques used to form nonradiative defects and their impact on nonsaturable loss.

4.1.2 Formation of nonradiative defects

One way to speed up the recombination processes is to incorporate a large density of deep level traps in a semiconductor [13]. Trapping of carriers into deep levels can proceed on sub-picosecond time scales as schematically shown in Fig. 11. In this figure, we distinguish the thermalization and the recombination at two different timescales; the carriers thermalize and form a thermal equilibrium on a 100 fs time scale, while carrier trapping proceeds on times scales from a few hundreds of femtoseconds to tens of picoseconds depending on the mobility of the carriers and the defect density. Higher defect densities give rise to faster trapping.

To generate mid-band gap defect-induced states in the absorber material, different approaches have been used including ion irradiation, deep impurity doping, low-temperature epitaxial growth, or a combination of doping and low-temperature epitaxial growth.

1) Ion-irradiation. Ion irradiation is a kind of ex-situ treatment. This technique consists in bombarding the semiconductor structure with ions of very high energies. Ions will thus pass through the active layer from one side and create defects throughout their passage. Many ions have been studied in the framework of the development of this technique. The use of light ions such as protons (H^+) will create point defects [51], while the use of heavy ions such as nickel (Ni^+) [52], gold (Au^+) or the oxygen (O^+) [53] will create many defects in the form of aggregates. Although both types of ions have been used to obtain relaxation times of a few picoseconds, the heavy ions give shorter recovery time and more created defects, and are less sensitive to temperature [54]. Finally, it should be noted that the exciton absorption, although slightly degraded, is still visible for radiation doses up to $1\times 10^{12}\,cm^{-2}$ [53]. Unfortunately, this technique has a significant effect on the reflectivity of the SESAM, which is due to the introduction of optical losses in the Bragg layers related to the irradiation step [55]. The reflectivity maybe reduced down to 98% that is 2% equivalent cavity losses, which is generally not adapted to VECSEL operation at 1.55 μm considering the available gain.

2) Low-temperature epitaxial growth. Most of optoelectronic components based on semiconductor material require high structural quality, hence require to grow the semiconductor layers at typical temperatures of 500°C to 600°C for MBE [56]. By decreasing the growth temperature, many microscopic structural defects appear (excess of as antisite as for example in GaAs) and form deep levels traps that capture the excited carriers [57]. Experience shows that the carrier relaxation time decreases with growth temperature. Thus sub-picosecond carrier relaxation times were achieved with quantum wells on GaAs

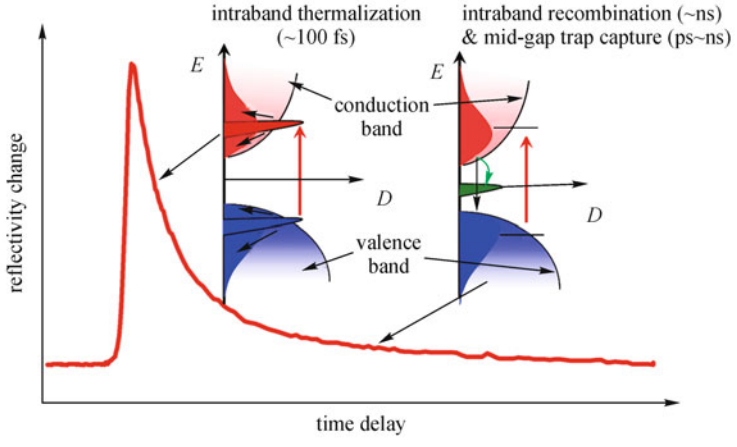

Fig. 11 Carrier dynamics in SESAMs: Electrons are excited to the conduction band and thermalize on a time scale of 100 fs. The electrons then recombine or get trapped by defects on a time scale of 0.1–100 ps [13]

[58–60] and on InP (but associated with doping) [61] for growth temperatures of 310°C and 200°C respectively.

3) Deep impurity doping. This technique allows for the creation of non-radiative recombination centers during material growth. To date, two elements were mainly used to reduce the recovery time: beryllium (Be) and iron (Fe). Doping with Be is always associated with a low-temperature growth [61,62]. In addition to the defects associated with low growth temperature, the Be atoms form complexes with As in GaAs based materials which act as centers of capture and recombination of carriers. Doping with Fe is performed at a higher growth temperature (~ 450°C). The Fe atoms replace the In in the crystal lattice and thus form deep acceptor levels which will trap the carriers [63]. In both cases, the carrier relaxation time decreases with the doping density. The technique of Be doping has allowed to achieve a relaxation time as short as 250 fs for GaAs/AlAs quantum wells (doping concentration of $2\times10^{19}\,\mathrm{cm^{-3}}$ and growth temperature of 280°C) [62] and 1 ps for InGaAs/InAlAs quantum wells (doping concentration of $7.8\times10^{17}\,\mathrm{cm^{-3}}$ and growth temperature of 200°C) [61]. The Fe doping technique has resulted in a recovery time of 290 fs for InGaAs/InP quantum wells (concentration of $2\times10^{19}\,\mathrm{cm^{-3}}$) [64].

These techniques we have mentioned, allow to obtain recovery time short enough to obtain a passive mode locking with ultra-short pulses (<250 ps). Unfortunately, the temporal response was accelerated at the expense of high nonsaturable losses preventing the SESAM to be used in a VECSEL cavity.

Within the last decade, dilute nitride alloys have attracted considerable interest due to their strong ability in decreasing the band gap of GaAs-based material [65,66]. It has also been early established that the addition of nitrogen (N) shortens the carrier lifetime of as-grown III-V alloys, due to the presence of traps and nonradiative centers. Härkönen et al. at Tampere University of Technology have studied the dynamics of a GaInNAs SESAM and have measured relaxation times of 30–40 ps for an as-grown structure with N compositions ranging from 1% to 3.5% [67]. To lower this time to a few picoseconds, additional recombination centers need to be introduced. However, a further increase of the N content in the quantum well would also result in a drastic change of its absorption characteristics: a redshift and a significant broadening of the absorption edge are observed.

Le Dû et al. at LPN used very thin N-rich GaNAs layers (containing a high amount of nitrogen (N)) in order to reduce the carrier recovery time [68]. In Fig. 12, we can see the GaNAs layers are placed very close to the quantum well (a few nanometers) to enable carriers to be evacuated by the tunnel effect and then to recombine. The carrier relaxation time may be adjusted by the thickness of the GaAs spacer separating the quantum well and GaAsN plane. This approach avoids the need for increasing too much the N-content in the quantum wells itself. It was used to fabricate microcavities with InGaNAs or InGaNAsSb quantum wells on GaAs substrates. One of these structures operating at 1.55 μm has yielded a recovery time down to a few tens of picoseconds [69]. To reduce the recombination time, it is important to obtain a high concentration of nitrogen in the GaAsN recombination plane (~ 10%). Among the techniques mentioned above, the use of nitrogen planes is a technique that induces less deterioration in the optical quality of the quantum wells and of the SESAM structure as a whole. The carrier recovery time may be controlled by the distance between the planes of nitrogen and the quantum wells, by the number of inserted planes, as well as by the nitrogen concentration in the planes. In addition, we can hope to vary the recovery time from several tens of picoseconds to less than ten picoseconds. Moreover, the absorber is grown on a GaAs substrate, this allows us to grow broadband AlAs/GaAs Bragg mirror as the bottom mirror. In our work, we have followed this technique for the fabrication of SESAM operating at 1.55 μm with fast carrier recovery time while maintaining a low non-saturated loss ($<0.5\%$).

4.2 SESAM design and fabrication

The SESAM structures were grown by MBE on a GaAs substrate and consisted of a 35-pair GaAs/AlAs Bragg mirror and a GaAs layer including the absorbing region. For the absorbing region, we used InGaNAsSb quantum well surrounded on both sides by one GaAsN fast recombination planes at a distance of 1 nm, as schematically depicted in Fig. 12. Figure 13 shows the experimental results fitted by a double exponential curve for the SESAMs, the fast component of carrier recovery time τ_1 is of 5 ps for the SESAMs thanks to fast tunnelling and recombination into the GaAsN planes. In Fig. 13, the pedestal at small negative delay is due to a residual pump

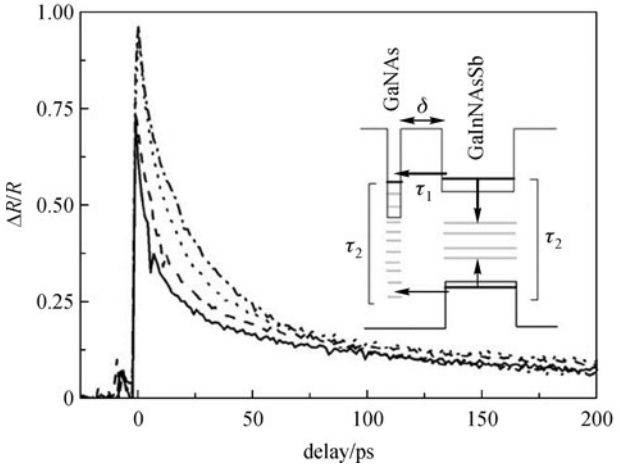

Fig. 12 Schematic diagram with recombination scheme using N-rich GaNAs layers as recombination center [69]

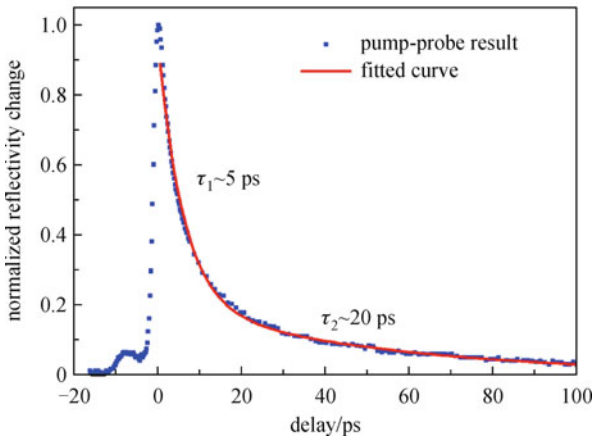

Fig. 13 Nonlinear reflectivities of SESAM as function of time delay between pump and probe pulse (The pulse duration of pump and probe signal is ~ 1.5 ps)

pulse preceding the main one. Due to its small amplitude, it does not affect the measured absorption recovery time values.

In Fig. 14, the SESAM structure was designed to allow for a precise adjustment of the group dispersion delay. To obtain this, top phase layers of GaAs and $Al_{0.7}Ga_{0.3}As$ were alternatively grown above the absorbing region, so that citric acid solution/diluted HF could be used to selectively etch the GaAs/$Al_{0.7}Ga_{0.3}As$ phase layers. By removing one or several of these layers, the microcavity resonance was modified (the microcavity could be tuned from resonant to antiresonant configuration at the wavelength of 1.55 μm). As a consequence, the group delay dispersion (GDD) value was also modified. The advantage of this design is that the carrier recovery time (another key parameter for short pulse generation) was kept constant during the tuning procedure, so that all the cases from anti-resonant to resonant could be covered by the cavity mode, with a controlled GDD value.

The as-grown SESAM structure was designed to present an anti-resonant configuration at 1.55 μm. The phase layers could first be etched to obtain a resonant configuration. Starting from the resonant configuration, two methods were employed to achieve a SESAM configuration showing low unsaturable loss but still large enough modulation depth for mode-locking, as will be further detailed in Section 5.2. In configuration A, a SiO_2 layer (nominal thickness of 277 nm, and refractive index of ~1.46 at 1.56 μm), acting as a partial AR coating, was deposited by plasma enhanced chemical vapor deposition (PECVD) on the surface of the resonant SESAM. In configuration B, selective etching of one more phase layer was performed. The top phase layers of the four types of SESAMs are described in Table 3.

The SESAMs were characterized by measuring their nonlinear reflectivity, where a laser source operating at 1550 nm with pulse width of 1.5 ps was used in the pump-probe system. The different resulting modulation depths ΔR and the saturation fluences F_{sat} are shown in Fig. 15 and presented in Table 3. The results indicate that type-B SESAM is an intermediate case between the resonant and type-A configurations. Type-B SESAM shows a modulation depth between the two other values, while the saturation fluences are nearly at the same level of ~10 μJ/cm^2 for the three cases. The estimated values of F_{sat} and ΔR for the anti-resonant SESAM are also given in the table: a larger value of F_{sat} and a small ΔR is obtained compared to the three other cases. To further describe the type-A and type-B SESAMs, the experimental reflectivity spectra and the corresponding GDD values (calculated with a transfer matrix model) are shown in Fig. 16. The type-A SESAM shows a flat-top reflectivity spectrum with a small reflectivity contrast indicating a relatively low

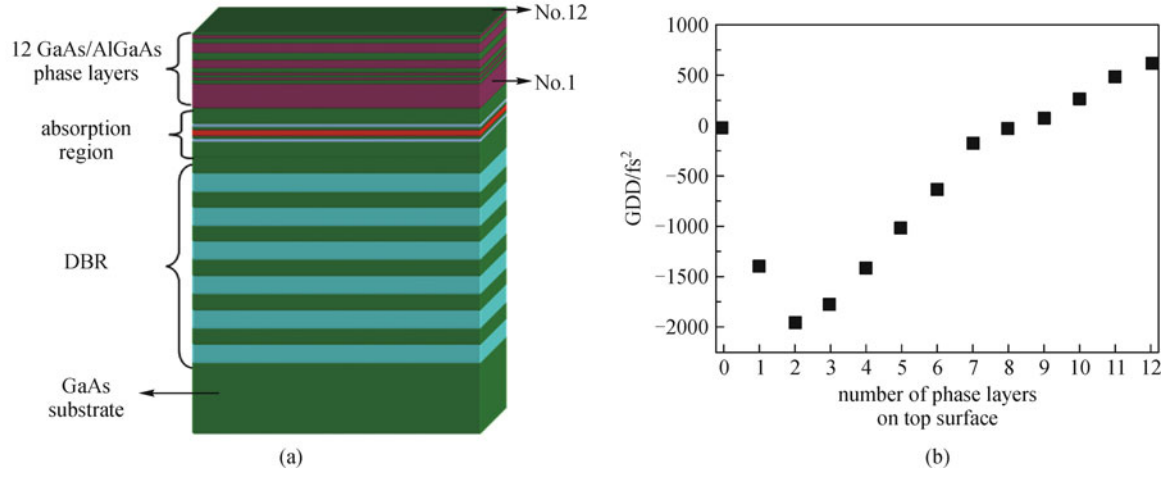

Fig. 14 Illustration of design of SESAM. (a) Schematic overview of the whole structure of SESAM, a quantum well surrounded by two GaNAs planes of absorption region and top phase layers of GaAs and $Al_{0.7}Ga_{0.3}As$ were grown alternatively; (b) calculated GDD of the SESAM as function of the number of phase layers on top of absorbing region

Table 3 Nominal thickness of top layers and measured nonlinear parameters of SESAM in the four configurations. Values in brackets are estimated from a transfer matrix calculation (from Ref. [70])

		resonant	type A	type B	anti-resonant
layer nominal thickness/nm	SiO_2	×	277	×	×
	GaAs	9.1	9.1	×	×
	$Al_{0.7}Ga_{0.3}As$	140.0	140.0	140.0	×
$F_{sat}/(\mu J \cdot cm^{-2})$		7.2	13.7	10.1	(63)
$\Delta R/\%$		3.4	1.6	2.4	(0.42)

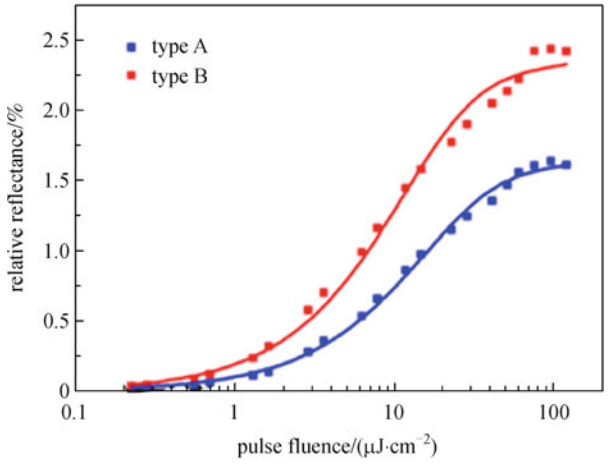

Fig. 15 Measured nonlinear reflectivities of SESAMs type A (blue squares) and type B (red squares). The red and blue lines are the corresponding fitting curves

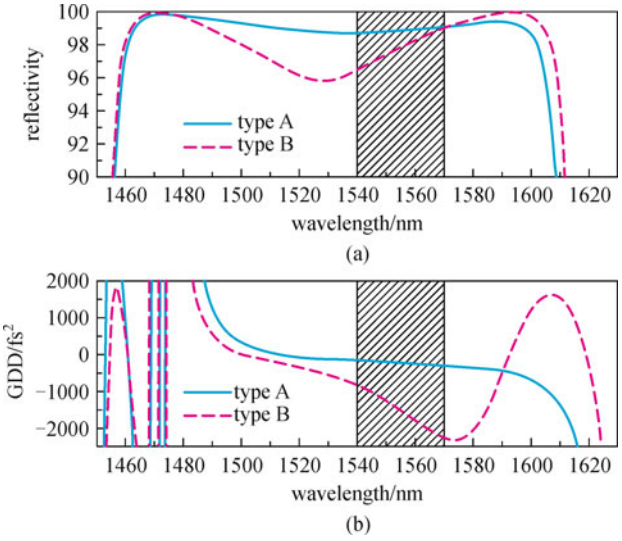

Fig. 16 (a) Experimental reflectivity of type A SESAM (blue curve) and type B SESAM (red dash); (b) corresponding calculated GDD value of the two SESAMs (from Ref. [70])

modulation depth. The calculated GDD value was -200 fs^2 with a variation of ± 50 fs^2 in the operation region (gray area). In case B, the microcavity resonance was shifted to 1.52 μm. This detuned resonant configuration corresponds to a larger modulation depth and a calculated GDD value of -2000 fs^2 at the lasing wavelength of ~1.56 μm.

5 Mode-locking experiments

5.1 Four-mirror cavity

The VECSEL chip and the SESAM can be considered as plane mirrors from a geometrical point of view. To achieve the regime of passive mode locking, the gain in the active structure must be sufficient to allow the pulse intensity on the SESAM to be greater than the absorber saturation intensity. The cavities used for passive mode-locking contain several optical elements, often concave mirrors, allowing changing the size of the waist of the fundamental mode on the SESAM and the VECSEL structure. This type of cavities containing several elements has been a subject of numerous publications dealing with the analysis and compensation for the astigmatism generated at the cavity output [71–73]. To select the cavity configuration appropriate to achieve passive mode locking, there are several parameters to be taken into account: 1) the length of the cavity, which is connected to the repetition rate; 2) the cavity mode size on the SESAM and VECSEL mirrors must ensure that the mode area ratio A_g/A_a can be adjusted to a value typically between 10 and 30 for stable mode locking [26].

Figure 17 depicts the cavity configuration which was assembled for the mode-locking experiments. This configuration has several advantages, either for the gain point of view (the pulse passes twice on the structure VECSEL and once on the SESAM in each round-trip in the cavity), or from the geometric point of view because we can control the cavity mode size of the SESAM and the VECSEL structure independently by adjusting the arm lengths d_S and d_V.

After optical design optimization, the parameters in the Z-cavity that have been used in this work are as follows:

1) Radius of curvature of output coupling mirror R = 25 mm.

2) Radius of curvature of folding mirror R = 18 mm.

3) Overall cavity length of 75 mm ($d_s + d_M + d_V \approx$ 75 mm), for operation at 2 GHz frequency. The arm length

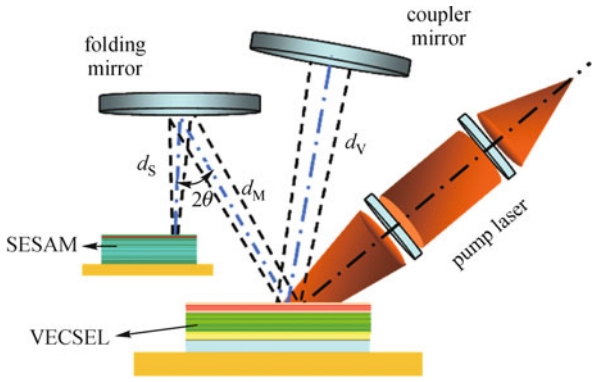

Fig. 17 Four-mirror cavity configuration of mode-locked VECSEL

d_s is ~11 mm and d_V is ~ 25 mm, which gives the ratio between the mode sizes on the VECSEL and SESAM of typically ~5.

4) Multimode pump laser, maximum pump power up to 8 W and pump spot ~100 μm × 120 μm.

The VECSEL with CVD diamond substrate was assembled with a fast SESAM in a four-mirror cavity schematically depicted in Fig. 17. To approach the optimal mode-locked pulse parameters and achieve the shortest pulsewidth, the SESAM structure was specifically designed to allow for a step-by-step tuning of the SESAM microcavity resonance, and therefore a modification of the modulation depth and GDD, as described in the preceding section.

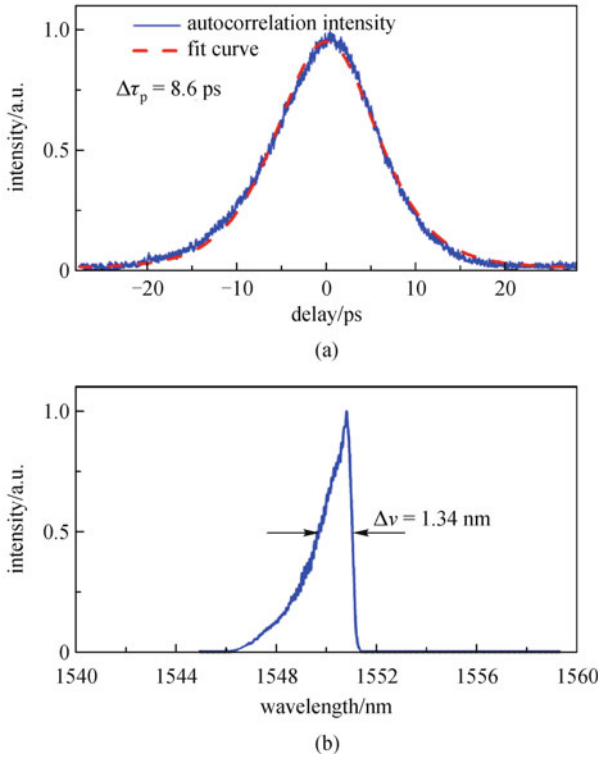

Fig. 18 (a) Autocorrelation trace of the mode-locked pulse obtained for type-A SESAM. Blue curve: experimental data. Red dash: fit assuming a sech^2 pulse; (b) corresponding average optical spectrum (from Ref. [70])

5.2 From picosecond to sub-picosecond pulse duration

The VECSEL with CVD diamond substrate was assembled with a fast SESAM in a four-mirror cavity schematically depicted in Fig. 17. We first found that the modulation depth of the single quantum well SESAM in anti-resonant configuration (at lasing wavelength) was low in that case and did not allow to achieve mode-locking operation, while CW operation dominated. By contrast, when the phase layers were etched to reach a resonant configuration at lasing wavelength, no lasing was actually observed due to too much absorption. On the other hand, stable mode-locking operation was established with both SESAMs type-A and type-B at the fundamental repetition frequency of ~ 2 GHz, by tuning the arm length d_s (see Fig. 17) around its optimal value of ~11 mm in order to minimize the spot size on the SESAM structure. The mode-locking regime was said to be stable if the radio frequency (RF)-linewidth (measured at the fundamental frequency) of the free-running laser was found to be narrower than ~ 1 kHz, with a stable RF spectrum.

With the type-A SESAM, we obtained stable mode-locked pulses of 8.6 ps duration with a narrow spectral width of 1.34 nm, as seen in Fig. 18. A sharp decay in optical spectrum at 1550 nm was observed similar to the result of Lindberg et al. [29], presumably due to the variation of dispersion in the gain chip assembly. The maximum average power was ~24 mW at output coupling mirror when the incident pump power was 2.9 W. It should be noted that a similar power is coupled out of the cavity at the folding mirror. When we changed to type-B SESAM, a stable mode-locked pulse with a width of ~ 900 fs was obtained. The spectro-temporal characteristics of the pulsed emission are displayed in Fig. 19. The background in the autocorrelation trace of Fig. 19(a) is due to the dark current of the photomultiplier used to detect the second harmonic signal. The pulsewidth deduced from the autocorrelation trace is 902 fs, assuming a sech^2 pulse. The maximum average optical power was measured to be 10 mW at the output coupling mirror under pump power of 2.5 W. The corresponding time-bandwidth product is of 0.36, which is 1.14 times the Fourier-transform limit. This is the shortest pulsewidth reported to our knowledge from a 1.56 μm ML-VECSEL. The gray area in Fig. 16 shows the wavelength region where stable mode-locking was obtained for SESAMS type-A and type-B. From Fig. 16, configuration B corresponded to a larger modulation depth and a GDD value of $-2000\ \text{fs}^2$ at 1.56 μm. It was experimentally reported that a slightly positive intracavity GDD should lead to shorter pulses in a soliton-like mode-

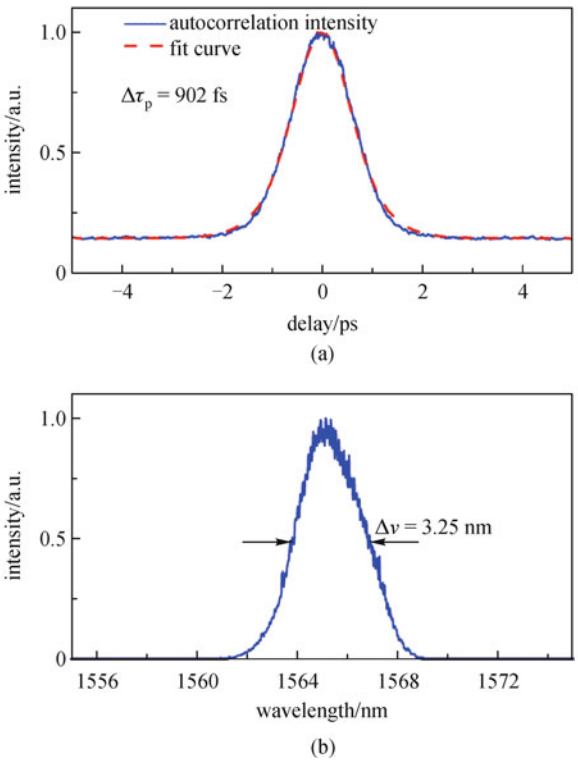

Fig. 19 (a) Autocorrelation trace of the mode-locked pulse obtained for type-B SESAM. Blue curve: experimental data. Red dash: fit assuming a sech^2 pulse; (b) corresponding average optical spectrum (from Ref. [70])

locking [74,75]. However, we could not get a reliable estimate of our VECSEL chip GDD, and hence of the total cavity GDD leading to the shortest pulsewidth.

6 Conclusions and outlook

ML-VECSELs show very attractive performance in power scaling capability, ultrashort pulse generation at high repetition rate with great wavelength versatility. Owing to these advantageous features, researchers have put intense efforts into the development of such vertical-cavity based short pulse source in the last decades. ML-VECSELs at 1.55 μm generating high power ultrashort pulse at high repetition rates can be a promising pulse source in telecommunication system. However, the common challenges for this family of pulse sources are to dissipate the heat originating from photo-absorption in InP based gain structure efficiently and to develop fast SESAM with proper properties at 1.55 μm. In this paper, we reviewed the main advances in thermal optimization of optically-pumped VECSEL for high output power operation at 1.55 μm. In downward heat sinking approach, VECSELs with a low thermal resistance are fabricated using a hybrid metal-metamorphic GaAs/AlAs mirror and bonding to a highly thermally conductive host substrate. The VECSEL chip assembled with a 1.55 μm fast InGaAs(Sb)N/GaAsN SESAM produces nearly Fourier transform-limited mode-locked pulses at ~ 2 GHz repetition frequency. When the resonance and GDD of the SESAM microcavity are tuned by selective etching of specific top phase layers, the mode-locked pulse width is reduced from several picoseconds to less than 1 ps. Shorter pulses may be expected with a finer control of the cavity resonance thanks to systematic selective etching of phase layers with optimized design of both VECSEL and SESAM chips in the mode-locking cavity.

Acknowledgements The authors thank Dr. Jean Decobert of Alcatel Thales 3-5lab for fruitful discussions and for the epitaxy of the InP-based active region in the VECSEL structure. Part of this work has been funded by Agence Nationale de la Recherche (ANR) in the framework of TONICS project. Z. Zhao was financially supported by China Scholarship Council for this work. LPN is a member of RENATECH national network of large micro-nanofabrication facilities.

References

1. Mollenauer L F, Mamyshev P V, Gripp J, Neubelt M J, Mamysheva N, Grüner-Nielsen L, Veng T. Demonstration of massive wavelength-division multiplexing over transoceanic distances by use of dispersion-managed solitons. Optics Letters, 2000, 25(10): 704–706.
2. Miller D A B. Rationale and challenges for optical interconnects to electronic chips. Proceedings of the IEEE, 2000, 88(6): 728–749
3. Mule A V, Glytsis E N, Gaylord T K, Meindl J D. Electrical and optical clock distribution networks for gigascale microprocessors. IEEE Transactions on Very Large Scale Integration (VLSI) Systems, 2002, 10(5): 582–594
4. Aisawa S, Sakamoto T, Fukui M, Kani J, Jinno M, Oguchi K. Ultra-wideband, long distance WDM demonstration of 1 Tbit/s (50×20 Gbit/s) 600 km transmission using 1550 and 1580 nm wavelength bands. Electronics Letters, 1998, 34(11): 1127–1128
5. Keeler G A, Nelson B E, Agarwal D, Debaes C, Helman N C, Bhatnagar A, Miller D A B. The benefits of ultrashort optical pulses in optically interconnected systems. IEEE Journal on Selected Topics in Quantum Electronics, 2003, 9(2): 477–485
6. Juodawlkis P W, Twichell J C, Betts G E, Hargreaves J J, Younger R D, Wasserman J L, O'Donnell F J, Ray K G, Williamson R C. Optically sampled analog-to-digital converters. IEEE Transactions on Microwave Theory and Techniques, 2001, 49(10): 1840–1853
7. Lau K Y, Ury I, Yariv A. Passive and active mode locking of a semiconductor laser without an external cavity. Applied Physics Letters, 1985, 46(12): 1117–1119
8. Hou L, Haji M, Akbar J, Qiu B, Bryce A C. Low divergence angle and low jitter 40 GHz AlGaInAs/InP 1.55 μm mode-locked lasers. Optics Letters, 2011, 36(6): 966–968
9. Merghem K, Akrout A, Martinez A, Aubin G, Ramdane A, Lelarge F, Duan G H. Pulse generation at 346 GHz using a passively mode locked quantum-dash-based laser at 1.55 μm. Applied Physics

Letters, 2009, 94(2): 021107-1–021107-3
10. Nakazawa M, Yamamoto T, Tamura K R. 1.28 Tbit/s-70 km OTDM transmission using third- and fourth-order simultaneous dispersion compensation with a phase modulator. Electronics Letters, 2000, 36 (24): 2027–2029
11. Xu C, Liu X, Mollenauer L F, Wei X. Comparison of return-to-zero differential phase-shift keying and ON-OFF keying in long-haul dispersion managed transmission. IEEE Photonics Technology Letters, 2003, 15(4): 617–619
12. Martinez A, Yamashita S. Multi-gigahertz repetition rate passively modelocked fiber lasers using carbon nanotubes. Optics Express, 2011, 19(7): 6155–6163
13. Keller U, Tropper A C. Passively modelocked surface-emitting semiconductor lasers. Physics Reports, 2006, 429(2): 67–120
14. Oehler A E H, Südmeyer T, Weingarten K J, Keller U. 100 GHz passively mode-locked Er:Yb:glass laser at 1.5 μm with 1.6-ps pulses. Optics Express, 2008, 16(26): 21930–21935
15. Hoogland S, Dhanjal S, Tropper A C, Roberts J S, Häring R, Paschotta R, Morier-Genoud F, Keller U. Passively mode-locked diode-pumped surface-emitting semiconductor laser. IEEE Photonics Technology Letters, 2000, 12(9): 1135–1137
16. Wilcox K G, Quarterman A H, Apostolopoulos V, Beere H E, Farrer I, Ritchie D A, Tropper A C. 175 GHz, 400-fs-pulse harmonically mode-locked surface emitting semiconductor laser. Optics Express, 2012, 20(7): 7040–7045
17. Quarterman A H, Wilcox K G, Apostolopoulos V, Mihoubi Z, Elsmere S P, Farrer I, Ritchie D A, Tropper A C. A passively mode-locked external-cavity semiconductor laser emitting 60-fs pulses. Nature Photonics, 2009, 3(12): 729–731
18. Rudin B, Wittwer V J, Maas D J H C, Hoffmann M, Sieber O D, Barbarin Y, Golling M, Südmeyer T, Keller U. High-power MIXSEL: an integrated ultrafast semiconductor laser with 6.4 W average power. Optics Express, 2010, 18(26): 27582–27588
19. Wilcox K G, Quarterman A H, Beere H, Ritchie D A, Tropper A C. High peak power femtosecond pulse passively mode-locked vertical-external-cavity surface-emitting laser. IEEE Photonics Technology Letters, 2010, 22(14): 1021–1023
20. Garnache A, Hoogland S, Tropper A C, Sagnes I, Saint-Girons G, Roberts J S. Sub-500-fs soliton pulse in a passively mode-locked broadband surface-emitting laser with 100-mW average power. Applied Physics Letters, 2002, 80(21): 3892–3894
21. Klopp P, Griebner U, Zorn M, Klehr A, Liero A, Weyers M, Erbert G. Mode-locked InGaAs-AlGaAs disk laser generating sub-200-fs pulses, pulse picking and amplification by a tapered diode amplifier. Optics Express, 2009, 17(13): 10820–10834
22. Aschwanden A, Lorenser D, Unold H J, Paschotta R, Gini E, Keller U. 2.1-W picosecond passively mode-locked external-cavity semiconductor laser. Optics Letters, 2005, 30(3): 272–274
23. Haring R, Paschotta R, Aschwanden A, Gini E, Morier-Genoud F, Keller U. High-power passively mode-locked semiconductor lasers. IEEE Journal of Quantum Electronics, 2002, 38(9): 1268–1275
24. Hoogland S, Garnache A, Sagnes I, Roberts J S, Tropper A C. 10-GHz train of sub-500-fs optical soliton-like pulses from a surface-emitting semiconductor laser. IEEE Photonics Technology Letters, 2005, 17(2): 267–269
25. Aschwanden A, Lorenser D, Unold H J, Paschotta R, Gini E, Keller U. 10-GHz passively mode-locked surface emitting semiconductor laser with 1.4-W average output power. Applied Physics Letters, 2005, 86(13): 131102-1–131102-33
26. Lorenser D, Unold H J, Maas D J H C, Aschwanden A, Grange R, Paschotta R, Ebling D, Gini E, Keller U. Towards wafer-scale integration of high repetition rate passively modelocked surface-emitting semiconductor lasers. Applied Physics B, Lasers and Optics, 2004, 79(8): 927–932
27. Lorenser D, Maas D J H C, Unold H J, Bellancourt A R, Rudin B, Gini E, Ebling D, Keller U. 50-GHz passively mode-locked surface-emitting semiconductor laser with 100 mW average output power. IEEE Journal of Quantum Electronics, 2006, 42(8): 838–847
28. Hoogland S, Garnache A, Sagnes I, Paldus B, Weingarten K J, Grange R, Haiml M, Paschotta R, Keller U, Tropper A C. Picosecond pulse generation with 1.5 μm passively modelocked surface-emitting semiconductor laser. Electronics Letters, 2003, 39 (11): 846–847
29. Lindberg H, Sadeghi M, Westlund M, Wang S M, Larsson A, Strassner M, Marcinkevicius S. Mode locking a 1550 nm semiconductor disk laser by using a GaInNAs saturable absorber. Optics Letters, 2005, 30(20): 2793–2795
30. Saarinen E J, Puustinen J, Sirbu A, Mereuta A, Caliman A, Kapon E, Okhotnikov O G. Power-scalable 1.57 μm mode-locked semiconductor disk laser using wafer fusion. Optics Letters, 2009, 34(20): 3139–3141
31. Khadour A, Bouchoule S, Aubin G, Harmand J C, Decobert J, Oudar J L. Ultrashort pulse generation from 1.56 μm mode-locked VECSEL at room temperature. Optics Express, 2010, 18(19): 19902–19913
32. Kuznetsov M. VECSEL Semiconductor Lasers: A Path to High-Power, Quality Beam and UV to IR Wavelength by Design. In: Okhotnikov O G, ed. Semiconductor Disk Lasers: Physics and Technology. Weinheim: Wiley-VCH Verlag GmbH & Co. KGaA, 2010
33. Rudin B, Rutz A, Hoffmann M, Maas D J H C, Bellancourt A R, Gini E, Südmeyer T, Keller U. Highly efficient optically pumped vertical-emitting semiconductor laser with more than 20 W average output power in a fundamental transverse mode. Optics Letters, 2008, 33(22): 2719–2721
34. Lindberg H, Strassner M, Bengtsson J, Larsson A. InP-based optically pumped VECSEL operating CW at 1550 nm. IEEE Photonics Technology Letters, 2004, 16(2): 362–364
35. Lindberg H, Strassner M, Gerster E, Larsson A. 0.8 W optically pumped vertical external cavity surface emitting laser operating CW at 1550 nm. Electronics Letters, 2004, 40(10): 601–602
36. Rautiainen J, Lyytikäinen J, Sirbu A, Mereuta A, Caliman A, Kapon E, Okhotnikov O G. 2.6 W optically-pumped semiconductor disk laser operating at 1.57-μm using wafer fusion. Optics Express, 2008, 16(26): 21881–21886
37. Tourrenc J P, Bouchoule S, Khadour A, Harmand J C, Decobert J, Lagay N, Lafosse X, Sagnes I, Leroy L, Oudar J L. Thermal optimization of 1.55 μm OP-VECSEL with hybrid metal-metamorphic mirror for single-mode high power operation. Optical and Quantum Electronics, 2008, 40(2–4): 155–165

38. Lindberg H, Strassner M, Bengtsson J, Larsson A. High-power optically pumped 1550-nm VECSEL with a bonded silicon heat spreader. IEEE Photonics Technology Letters, 2004, 16(5): 1233–1235
39. Zhao Z, Bouchoule S, Ferlazzo L, Sirbu A, Mereuta A, Kapon E, Galopin E, Harmand J C, Decobert J, Oudar J L. Cost-effective thermally-managed 1.55-μm VECSEL with hybrid mirror on copper substrate. IEEE Journal of Quantum Electronics, 2012, 48(5): 643–650
40. Kemp A J, Valentine G J, Hopkins J M, Hastie J E, Smith S A, Calvez S, Dawson M D, Burns D. Thermal management in vertical-external-cavity surface-emitting lasers: finite-element analysis of a heatspreader approach. IEEE Journal of Quantum Electronics, 2005, 41(2): 148–155
41. Maclean A J, Birch R B, Roth P W, Kemp A J, Burns D. Limits on efficiency and power scaling in semiconductor disk lasers with diamond heatspreaders. Journal of the Optical Society of America B, Optical Physics, 2009, 26(12): 2228–2236
42. Lindberg H, Larsson A, Strassner M. Single-frequency operation of a high-power, long-wavelength semiconductor disk laser. Optics Letters, 2005, 30(17): 2260–2262
43. Bousseksou A, Bouchoule S, El Kurdi M, Strassner M, Sagnes I, Crozat P, Jacquet J. Fabrication and characterization of 1.55 μm single transverse mode large diameter electrically pumped VECSEL. Optical and Quantum Electronics, 2007, 38(15): 1269–1278
44. Caliman A, Mereuta A, Suruceanu G, Iakovlev V, Sirbu A, Kapon E. 8 mW fundamental mode output of wafer-fused VCSELs emitting in the 1550-nm band. Optics Express, 2011, 19(18): 16996–17001
45. Zhao Z, Bouchoule S, Galopin E, Ferlazzo L, Patriarche G, Harmand J C, Decobert J, Oudar J L. Thermal management in 1.55 μm InP-based VECSELs: heteroepitaxy of GaAs-based mirror and integration with electroplated substrate. In: French Symposium on Emerging Technologies for Micro- and Nano-fabrication, France, 2013
46. Paschotta R, Keller U. Passive mode locking with slow saturable absorbers. Applied Physics B, Lasers and Optics, 2001, 73(7): 653–662
47. Keller U. Ultrafast solid-state laser oscillators: a success story for the last 20 years with no end in sight. Applied Physics B, Lasers and Optics, 2010, 100(1): 15–25
48. Keller U, Knox W H, Roskos H. Coupled-cavity resonant passive mode-locked Ti: sapphire laser. Optics Letters, 1990, 15(23): 1377–1379
49. Keller U. Ultrafast all-solid state laser technology. Applied Physics B, Lasers and Optics, 1994, 58(5): 347–363
50. Haiml M, Siegner U, Morier-Genoud F, Keller U, Luysberg M, Lutz R C, Specht P, Weber E R. Optical nonlinearity in low-temperature-grown GaAs: microscopic limitations and optimization strategies. Applied Physics Letters, 1999, 74(21): 3134–3136
51. Lamprecht K F, Juen S, Palmetshofer L, Hopfel R A. Ultrashort carrier lifetimes in H^+ bombarded InP. Applied Physics Letters, 1991, 59(8): 926–928
52. Mangeney J, Choumane H, Patriarche G, Leroux G, Aubin G, Harmand J C, Oudar J L, Bernas H. Comparison of light- and heavy-ion-irradiated quantum-wells for use as ultrafast saturable absorbers. Applied Physics Letters, 2001, 79(17): 2722–2724
53. Lugagne Delpon E, Oudar J L, Bouché N, Raj R, Shen A, Stelmakh N, Lourtioz J M. Ultrafast excitonic saturable absorption in ion-implanted InGaAs/InAlAs multiple quantum wells. Applied Physics Letters, 1998, 72(7): 759–761
54. Joulaud L, Mangeney J, Lourtioz J M, Crozat P, Patriarche G. Thermal stability of ion irradiated InGaAs with (sub-) picosecond carrier lifetime. Applied Physics Letters, 2003, 82(6): 856–858
55. Khadour A. Source d'impulsions brèves à 1.55 μm en laser à cavité verticale externe pour application à l'échantillonnage optique linéaire. Dissertation for the Doctoral Degree. France: École Polytechnique, 2009
56. Gupta S, Whitaker J F, Mourou G A. Ultrafast carrier dynamics in III–V semiconductors grown by molecular-beam epitaxy at very low substrate temperatures. IEEE Journal of Quantum Electronics, 1992, 28(10): 2464–2472
57. Chin A, Chen W J, Ganikhanov F, Lin G R, Shieh J M, Pan C L, Hsieh K C. Microstructure and subpicosecond photoresponse in GaAs grown by molecular beam epitaxy at very low temperatures. Applied Physics Letters, 1996, 69(3): 397–399
58. Okuno T, Masumoto Y, Ito M, Okamoto H. Large optical nonlinearity and fast response time in low-temperature grown GaAs/AlAs multiple quantum wells. Applied Physics Letters, 2000, 77(1): 58–60
59. Gupta S, Frankel M Y, Valdmanis J A, Whitaker J F, Mourou G A, Smith F W, Calawa A R. Subpicosecond carrier lifetime in GaAs grown by molecular beam epitaxy at low temperatures. Applied Physics Letters, 1991, 59(25): 3276–3278
60. Harmon E S, Melloch M R, Woodall J M, Nolte D D, Otsuka N, Chang C L. Carrier lifetime versus anneal in low temperature growth GaAs. Applied Physics Letters, 1993, 63(16): 2248–2250
61. Takahashi R, Kawamura Y, Kagawa T, Iwamura H. Ultrafast 1.55-μm photoresponses in low-temperature-grown InGaAs/InAlAs quantum wells. Applied Physics Letters, 1994, 65(14): 1790–1792
62. Okuno T, Masumoto Y, Sakuma Y, Hayasaki Y, Okamoto H. Femtosecond response time in beryllium-doped low-temperature-grown GaAs/AlAs multiple quantum wells. Applied Physics Letters, 2001, 79(6): 764–766
63. Sderström D, Marcinkevicius S, Karlsson S, Lourdudoss S. Carrier trapping due to Fe^{3+}/Fe^{2+} in epitaxial InP. Applied Physics Letters, 1997, 70(25): 3374–3376
64. Gicquel-Guézo M, Loualiche S, Even J, Labbe C, Dehaese O, Le Corre A, Folliot H, Pellan Y. 290 fs switching time of Fe-doped quantum well saturable absorbers in a microcavity in 1.55 μm range. Applied Physics Letters, 2004, 85(24): 5926–5928
65. Kondow M, Uomi K, Hosomi K, Mozume T. Gas-source molecular beam epitaxy of GaN_xAs_{1-x} using a N radical as the N source. Japanese Journal of Applied Physics, 1994, 33(8A): L1056–L1058
66. Yang X, Héroux J B, Mei L F, Wang W I. InGaAsNSb/GaAs quantum wells for 1.55 μm lasers grown by molecular-beam epitaxy. Applied Physics Letters, 2001, 78(26): 4068–4070
67. Härkönen A, Jouhti T, Tkachenko N V, Lemmetyinen H, Ryvkin B, Okhotnikov O G, Sajavaara T, Keinonen J. Dynamics of photoluminescence in GaInNAs saturable absorber mirrors. Applied

Physics A, Materials Science & Processing, 2003, 77(7): 861–863
68. Le Dû M, Harmand J C, Meunier K, Patriarche G, Oudar J L. Growth of GaN_xAs_{1-x} atomic monolayers and their insertion in the vicinity of GaInAs quantum wells. IEE Proceedings- Optoelectronics, 2004, 151(5): 254–258
69. Dû M L, Harmand J C, Mauguin O, Largeau L, Travers L, Oudar J L. Quantum-well saturable absorber at 1.55 μm on GaAs substrate with a fast recombination rate. Applied Physics Letters, 2006, 88 (20): 201110-1–201110-3
70. Zhao Z, Bouchoule S, Song J Y, Galopin E, Harmand J C, Decobert J, Aubin G, Oudar J L. Subpicosecond pulse generation from a 1.56 μm mode-locked VECSEL. Optics Letters, 2011, 36(22): 4377– 4379
71. Cojocaru E, Julea T, Herisanu N. Stability and astigmatic compensation analysis of five- and six- or seven-mirror cavities for mode-locked dye lasers. Applied Optics, 1989, 28(13): 2577–2580
72. Li K K, Dienes A, Whinnery J R. Stability and astigmatic compensation analysis of five-mirror cavity for mode-locked dye lasers. Applied Optics, 1981, 20(3): 407–411
73. Anctil G, McCarthy N, Piché M. Sensitivity of a three-mirror cavity to thermal and nonlinear lensing: Gaussian-beam analysis. Applied Optics, 2000, 39(36): 6787–6798
74. Hoffmann M, Sieber O D, Maas D J H C, Wittwer V J, Golling M, Südmeyer T, Keller U. Experimental verification of soliton-like pulse-shaping mechanisms in passively modelocked VECSELs. Optics Express, 2010, 18(10): 10143–10153
75. Sieber O D, Hoffmann M, Wittwer V J, Mangold M, Golling M, Tilma B W, Südmeyer T, Keller U. Experimentally verified pulse formation model for high-power femtosecond VECSELs. Applied Physics B, Lasers and Optics, 2013, 113(1): 133–145

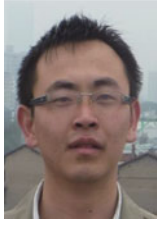

Zhuang Zhao received the B.Sc. degree in optical information science and technology from Harbin Engineering University, Harbin, China, in 2007 and the M.S. degree in optics engineering from Huazhong University of Science and Technology, Wuhan, China, in 2009. In 2012, he obtained his Ph.D. degree at the Laboratory for Photonics and Nanostructures/CNRS (France) for his work on short pulses generation from passive mode-locking optically pump vertical external cavity semiconductor lasers (OP-VECSELs). Currently, he works as a post-doctoral researcher at the Lasers Physics Laboratory/CNRS on laser diode pumped vertical external cavity organic lasers (VECSOL).

Sophie Bouchoule After her Ph.D. thesis on 1.55 μm semiconductor laser diodes, Dr. S. Bouchoule joined France Telecom-CNET laboratories, then OPTO + joint Alcatel-France Telecom Laboratory, where she was involved in the processing of high speed laser sources at 1550 nm for emerging 40 Gbit/s applications. In 2001, she joined CNRS, Laboratoire de Photonique et de Nanostructures (LPN), where she has been involved in the development of long-wavelength laser (V(E)CSEL) sources and III-V laser processing. Since 2007, she is also engaged in the development of semiconductor/organic UV-visible micocavity emitters. She is author or co-author of 80 papers in international journals and has contributed to more than 100 presentations at international conferences.

Jean-Christophe Harmand obtained his Ph.D. degree in physics at the University of Paris 7 (France) in 1988 for his work on GaAlAs/GaAs heterojunction bipolar transistors. From 1988 to 1990, he joined the Optoelectronic Research Laboratory of Matsushita in Osaka (Japan) as a post-doctoral researcher. There, he was involved in studies on metamorphic AlGaInAs/GaAs structures for high electron mobility transistors. In 1990, he joined the CNET/France Telecom R in Bagneux (France). From 1990 to 1999, he investigated growth by MBE of various III-V materials for optical telecommunication devices (laser, saturable absorbers, electro-optical modulators). In 1998, he obtained the "Habilitation à Diriger des Recherches" from University of Paris 7. In 1999, he entered the CNRS as a senior researcher in the Laboratory of Photonics and Nanostructures in Marcoussis (France). He coordinated several research activities in molecular beam epitaxy (MBE) growth including the fabrication of quantum confined structures (quantum wells, quantum dots and superlattices). He investigated III-V-N dilute nitride alloys for applications in optical fiber telecommunications. From 2004, he explored III-V nanowire growth by catalyst-assisted MBE. He is author and coauthor of 10 patents and about 250 publications in peer reviewed journal. He was awarded "Médaille d'Argent du CNRS" in 2012.

Gilles Patriarche obtained his Ph.D. in physics degree at Pierre et Marie Curie University (Paris) in 1992 for his works on epitaxy and crystal defects in the interfaces of II-VI semiconductor heterostructures grown on GaAs substrate. In 1993, he worked as a post-doctoral researcher in the Institut des matériaux de Nantes/CNRS. From 1994 to 1998, he took a post-doctoral position and then worked as senior scientist in the Research laboratory of France Telecom at Bagneux (CNET). In 1999, he entered the Laboratoire de Photonique et Nanostructures of the CNRS at Marcoussis as a senior scientist. In 2002, he obtained the "Habilitation à Diriger des Recherches" in physics from the Pierre et Marie Curie University, Paris. His current research interests are focused on the growth and the structural study of nanostructures of III-V semiconductors such as quantum dots, nanowires, multi-quantum wells and strained-layer superlattices. He is currently working on their chemical and structural characterization until the atomic scale, using Transmission Electron Microscopy and aberration corrected Scanning Transmission Electron Microscopy. Recent results have been obtained on the structural characterization and mechanisms growth of catalysed III-V nanowires, and the determination of the morphology and the

chemical composition of single InAsP Quantum Dot inserted in a nanowire. Other recent results of structural characterization have been obtained on the chemical composition and the strain field mapping of CdSe/CdZnS core/shells nanoplatelets. He works also on the structural characterization of III-V/Si heterostructures obtained by wafer bonding. He have authored and co-authored more than 380 journal papers (source ISI web of science) with a h-index of 34.

Guy Aubin received the B.S. degree from Ecole Nationale Supérieure des Télécommunications (ENST-Bretagne), Brest, France, and the M.S. degree in information processing from University of Rennes, Brest, France, both in 1981. He was the Head of Transmission Experimentation Group at the Submarine Networks Department of France Télécom R, Issy-les-Moulineaux, France, where he contributed to the world's first demonstration of 40 Gbit/s transmission over transoceanic distance, to the first trials of undersea optical amplified links and, well before, to the definition of first installed fibered systems. He is currently engaged at the Laboratory for Photonics and Nanostructures of the Centre National de la Recherche Scientifique, CNRS-LPN, Marcoussis, France since 2001. His research interests include new device functionalities for telecommunication systems. He is involved in the research on all-optical or opto-electronics function for next-generation networks and develops advanced demonstrating setups. He has authored or co-authored more than 120 research papers in international refereed journals and conference proceedings, and holds 3 patents in the test and measurement area.

Jean-Louis Oudar graduated at Ecole Polytechnique, Paris in 1971, and received the Doctorate ès-Sciences degree in physics in 1977 from the University of Paris. Performing research at CNET and later at France Telecom R, he has worked on nonlinear optical phenomena in condensed matter. Studying the enhanced optical nonlinearities of organic compounds, he developed the basis of a molecular engineering approach for nonlinear organic materials, an internationally recognised pioneering work. Since 2000, he works at the Laboratory for Photonics and Nanostructures of the Centre National de la Recherche Scientifique (CNRS-LPN). His present research interests include fast saturable absorber nanophotonic devices for all-optical regeneration, semiconductor light sources, short pulse generation and mode-locking phenomena in semiconductor lasers.